TASK QUARTERLY 12 No 3, 267–272

ROTATING RAYLEIGH-BENARD CONVECTION

WOJCIECH MAJCHROWSKI AND EWA TULISZKA-SZNITKO

Poznan University of Technology, Chair of Thermal Engineering,
Piotrowo 3, 60-965 Poznan, Poland
wojciech.majchrowski@doctorate.put.poznan.pl

(Received 12 May 2008)

Abstract: In the this paper our results on the natural convection in an enclosed rotating cavity are presented. We have focused our attention on the influence of the Rayleigh and Taylor numbers on the flow structure. DNS computations have been performed for the geometry of aspect ratio $L = 9$ and curvature parameter $\mathrm{Rm} = 1.5$.

Keywords: DNS, Rayleigh-Benard convection

1. Introduction

Rayleigh-Benard convection is a classical heat transport problem. An enclosed fluid layer is heated from below and cooled from above. Depending on the temperature difference $\Delta T^* = T_2^* - T_1^*$, different fluid behavior is observed. If the producing temperature difference exceeds the critical value of ΔT_c^*, this layer becomes unstable to buoyancy and a regular convection pattern appears. At even higher temperature differences, this regular pattern breaks down leading to plume dominated convective turbulence. The properties of this process have been studied by many authors: *e.g.* Rossby [1], Siggia [2]. Turbulent thermal convection appears in many technical applications, such as metal solidification processes or heat exchanger systems. When an additional factor such as rotation is included, the convection process complexity increases. The influence of rotation on the Rayleigh-Benard convection has been studied by many authors: *e.g.* Chandrasekhar [3, 4], Nagakawa and Frenzen [5], Rossby [1], Boubnov and Golistyn [6], Zhong *et al.* [7]. Processes of this kind are common in the world around us, we can observe it in fluid flow machineries, the Earth's atmosphere, the solid core of the Earth or in the Sun.

In order to investigate the properties of such configuration, and the transition to turbulence in particular, in this paper we investigate a uniformly rotating Boussinesq fluid bounded from above and below by horizontal rotating disks held at fixed temperatures. The geometrical model is described in Section 2. Sections 3 an 4 are devoted to the mathematical model and numerical approach, respectively.

2. Geometrical model

The geometrical domain is presented in Figure 1. The rotating (upper) disk rotates at uniform angular velocity Ω^*. The outer cylinder of radius R_1^* is attached to the stator and the inner cylinder of radius R_0^* is attached to the rotor. The geometrical shape is defined by dimensionless parameters: the curvature parameter Rm and the aspect ratio parameter L:

$$\begin{aligned} \mathrm{Rm} &= (R_1^* + R_0^*)/(R_1^* - R_0^*), \\ L &= (R_1^* - R_0^*)/2h^*. \end{aligned} \tag{1}$$

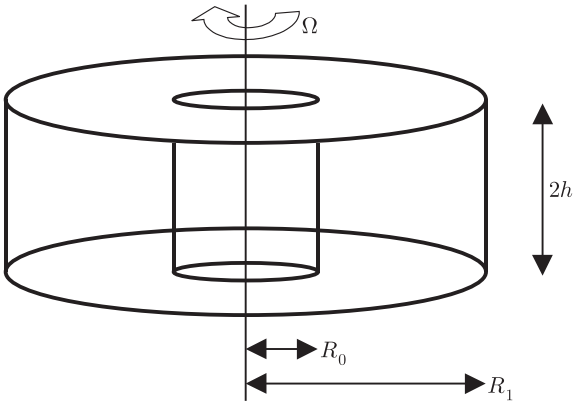

Figure 1. Geometrical model

The flow is controlled by the following physical parameters: the Rayleigh number, $\mathrm{Ra} = g^*\beta(T_2^* - T_1^*)(2h^*)^3/\nu^* a^*$, which denotes the respective relevance of buoyancy and dissipation, the Taylor number, $\mathrm{Ta} = (2\Omega^*(2h^*)^2/\nu^*)^2$, which defines rotation, the convective Rossby number, $\mathrm{Ro} = \sqrt{\mathrm{Ra}/(\mathrm{Ta}\cdot\mathrm{Pr})}$, which characterizes the respective importance of buoyancy and rotation, the Prandtl number, $\mathrm{Pr} = \nu^*/a^*$, which characterizes the dissipative properties of the fluid. In the above relations, β is the thermal expansion coefficient, T_1^* is the temperature of the upper rotating disk and inner cylinder and T_2^* indicates the temperature of the stator and outer cylinder, ν^* is the kinematics viscosity, g^* is the gravitational acceleration, $a^* = \lambda^*/\rho^* c_p^*$ is the thermal diffusivity (asterisk denotes dimensional value).

3. Mathematical model

The flow is described by continuity, Navier-Stokes and energy equations. The equations are written in a cylindrical coordinate system (r^*, φ, z^*), with respect to a rotating frame of reference. Time, length and velocity are normalized as follows: $(\Omega^*)^{-1}$, h^* and $\Omega^* R_1^*$. Radial and axial coordinates are normalized to interval $\langle -1;1\rangle$ by transformation:

$$r = \frac{2r^*}{R_1^* - R_0^*} - \mathrm{Rm} = \frac{r^*}{Lh^*} - \mathrm{Rm}, \quad z = \frac{z^*}{h^*}. \tag{2}$$

Normalization of variables is based on the free fall velocity $U^* = \sqrt{g^*\beta\Delta T^* 2h^*}$, as was proposed in [8]. We have introduced the dimensionless temperature defined as

follows: $\Theta = (T^* - T_1^*)/(T_2^* - T_1^*)$. After normalization, the governing equations can be written in the following form:

- Continuity equation:

$$\frac{1}{L}\frac{\partial u}{\partial r} + \frac{u}{(\mathrm{Rm}+r)L} + \frac{1}{(\mathrm{Rm}+r)L}\frac{\partial v}{\partial \varphi} + \frac{\partial w}{\partial z} = 0; \tag{3}$$

- Radial NS equation:

$$\frac{\partial u}{\partial t} + \frac{u}{L}\frac{\partial u}{\partial r} + \frac{v}{L(\mathrm{Rm}+r)}\frac{\partial u}{\partial \varphi} + w\frac{\partial u}{\partial z} - \frac{v^2}{L(\mathrm{Rm}+r)} - \sqrt{\frac{\mathrm{Pr\,Ta}}{4\mathrm{Ra}}}v - (r+\mathrm{Rm})L\frac{\mathrm{TaPr}}{16\mathrm{Ra}} =$$
$$-\frac{1}{L}\frac{\partial p}{\partial r} + 2\sqrt{\frac{\mathrm{Pr}}{\mathrm{Ra}}}\left[\frac{1}{L^2}\frac{\partial^2 u}{\partial r^2} + \frac{1}{(r+\mathrm{Rm})L^2}\frac{\partial u}{\partial r} + \frac{1}{(r+\mathrm{Rm})^2L^2}\frac{\partial^2 u}{\partial \varphi^2} + \right.$$
$$\left.\frac{\partial^2 u}{\partial z^2} - \frac{u}{L^2(\mathrm{Rm}+r)^2} - \frac{2}{L^2(\mathrm{Rm}+r)^2}\frac{\partial v}{\partial \varphi}\right]; \tag{4}$$

- Azimuthal NS equation:

$$\frac{\partial v}{\partial t} + \frac{u}{L}\frac{\partial v}{\partial r} + \frac{v}{(r+\mathrm{Rm})L}\frac{\partial v}{\partial \varphi} + w\frac{\partial v}{\partial z} + \frac{uv}{L(\mathrm{Rm}+r)} + \sqrt{\frac{\mathrm{TaPr}}{4\mathrm{Ra}}}u =$$
$$-\frac{1}{(r+\mathrm{Rm})}L\frac{\partial P}{\partial \varphi} + 2\sqrt{\frac{\mathrm{Pr}}{\mathrm{Ra}}}\left[\frac{1}{L^2}\frac{\partial^2 v}{\partial r^2} + \frac{1}{(r+\mathrm{Rm})L^2}\frac{\partial v}{\partial r} + \frac{1}{(r+\mathrm{Rm})^2L^2}\frac{\partial^2 v}{\partial \varphi^2} + \right.$$
$$\left.\frac{\partial^2 v}{\partial z^2} - \frac{v}{(r+\mathrm{Rm})^2L^2} + \frac{2}{(r+\mathrm{Rm})^2L^2}\frac{\partial u}{\partial \varphi}\right]; \tag{5}$$

- Axial NS equation:

$$\frac{\partial w}{\partial t} + \frac{u}{L}\frac{\partial w}{\partial r} + \frac{v}{(r+\mathrm{Rm})L}\frac{\partial w}{\partial \varphi} + w\frac{\partial w}{\partial z} = -\frac{\partial P}{\partial z} + \frac{1}{2}\Theta +$$
$$2\sqrt{\frac{\mathrm{Pr}}{\mathrm{Ra}}}\left[\frac{1}{L^2}\frac{\partial^2 w}{\partial r^2} + \frac{1}{(r+\mathrm{Rm})L^2}\frac{\partial w}{\partial r} + \frac{1}{(r+\mathrm{Rm})^2L^2}\frac{\partial^2 w}{\partial \varphi^2} + \frac{\partial^2 w}{\partial z^2}\right]; \tag{6}$$

- Energy equation:

$$\frac{\partial \Theta}{\partial t} + \frac{u}{L}\frac{\partial \Theta}{\partial r} + \frac{v}{(r+\mathrm{Rm})L}\frac{\partial \Theta}{\partial \varphi} + w\frac{\partial \Theta}{\partial z} =$$
$$\sqrt{\frac{4}{\mathrm{PrRa}}}\left[\frac{1}{L^2}\frac{\partial^2 \Theta}{\partial r^2} + \frac{1}{(r+\mathrm{Rm})L^2}\frac{\partial \Theta}{\partial r} + \frac{1}{(r+\mathrm{Rm})^2L^2}\frac{\partial^2 \Theta}{\partial \varphi^2} + \frac{\partial^2 \Theta}{\partial z^2}\right]. \tag{7}$$

The no-slip boundary condition is applied to all rigid walls, hence $u = w = 0$. The boundary conditions for the azimuthal velocity component are: $v = 0$ on the rotating disk, and $v = -(\mathrm{Rm}+r)/(\mathrm{Rm}+1)$ on the stator. The dimensionless temperature equals $\Theta = 0$ on the rotor and $\Theta = 1$ on the stator. Two different sets of temperature boundary conditions have been used on the cylinders – isothermal boundary conditions $\Theta = 0$ on the inner cylinder and $\Theta = 1$ on the outer cylinder or adiabatic boundary conditions $\partial\Theta/\partial n = 0$ on the cylinders.

4. Numerical approach

All the results are obtained by the Direct Numerical Simulation method (DNS) based on the pseudospectral collocation Chebyshev-Fourier method [9, 10]. The spatial approximation of the arbitrary dependent variable is as follows:

$$\Psi_{NMK}(r,z,\varphi,t) = \sum_{p=-K/2}^{K/2-1} \sum_{n=0}^{N} \sum_{m=0}^{M} \Psi_{nmp}(t)\; T_n(r)\; T_m(z)\; e^{ip\varphi}, \tag{8}$$

where t is dimensionless time, $T_n(r)$ and $T_m(z)$ are Chebyshev polynomials, $N+1$, $K+1$, $M+1$ are the numbers of grid points in radial, azimuthal and axial directions, respectively. The use of the Gauss-Lobatto collocation points in radial and axial directions ensures high accuracy of the solution inside the very narrow wall layers. The uniform mesh has been used in the azimuthal direction. The time derivative is approximated by a second order Euler backward scheme, the linear terms are implicitly evaluated at time $(n+1)t$, the non-linear part is explicitly evaluated at time $(n+1)t$ by means of Adams-Bashforth extrapolation. The solution is based on the predictor – corrector method and the matrix influence technique [9, 10].

5. Results

In the paper we present very preliminary results obtained by us for the rotating cavity of aspect ratio $L = 9$, curvature parameters $\mathrm{Rm} = 1.5$ and for the Rossby number $\mathrm{Ro} = 1$, 2 and 4. The main motivation of our work has been to compare different flow patterns affected by rotation and to verify our results by a qualitative comparison with similar results published in the literature [11–14]. A simulation was initialized with a zero meridian flow, a linear distribution of the azimuthal velocity component and a linear vertical temperature profile. Computations were performed at a constant Rosby number; with constant Ro we gradually increased the Rayleigh number Ra. The number of collocation points used in the radial, azimuthal and axial directions was $90 \times 90 \times 45$, respectively.

First, let us consider the isothermal condition on the end walls: $\Theta = 1$ at the outer cylinder and $\Theta = 0$ at the inner one. The meridian sections of the flow fields obtained for $\mathrm{Ra} = 10\,000$ are presented in Figures 2a, 2b and 2c for $\mathrm{Ro} = 1$, 2 and 4, respectively. For Ro=1 we observe a characteristic laminar flow structure, disturbed only near the end-wall cylinders. In Figure 2a we can see that fluid is pumped radially outward along the upper rotaing disk and recirculates along the bottom disc. With increasing Ro, the Rayleigh-Benard convection fluid flow patterns become stronger; for $\mathrm{Ro} = 4$ we have observed fully developed convection (Figure 2c). We have obtained a fully developed pattern of the flow for $\mathrm{Ro} = 1$ between 13 000 and 16 000, for $\mathrm{Ro} = 2$ between 10 000 and 13 000 and for $\mathrm{Ro} = 4$ between 7 000 and 10 000.

The time evolution of the azimuthal velocity component obtained for $\mathrm{Ro} = 1$ and $\mathrm{Ra} = 32\,000$, 44 000, 56 000 and 80 000 is presented in Figure 3. It can be seen in Figure 3 that the amplitudes of oscillations increase with increasing Ra.

We have obtained similar flow patterns to these presented in Figure 2 for the adiabatic boundary condition at the end-walls, however, this configuration has turned out to be more stable. The temperature field in the meridian sections obtained for

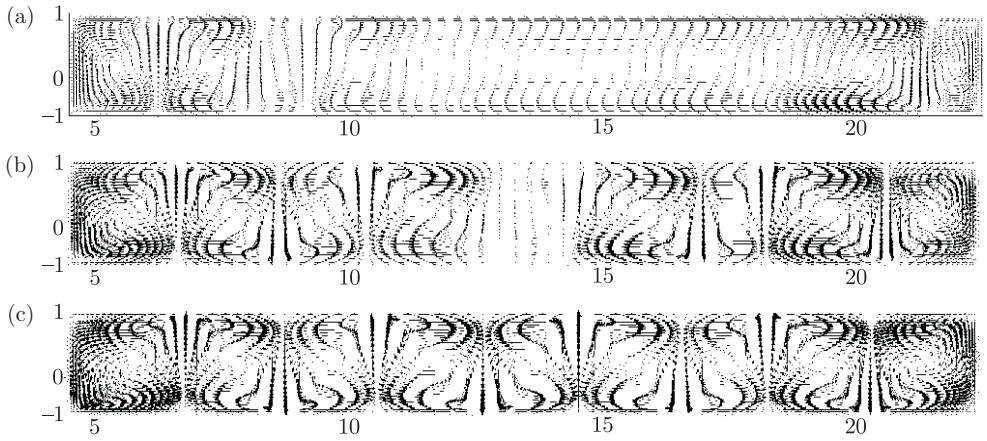

Figure 2. Velocity field meridial sections for Ra = 10 000: (a) Ro = 1, (b) Ro = 2, (c) Ro = 4

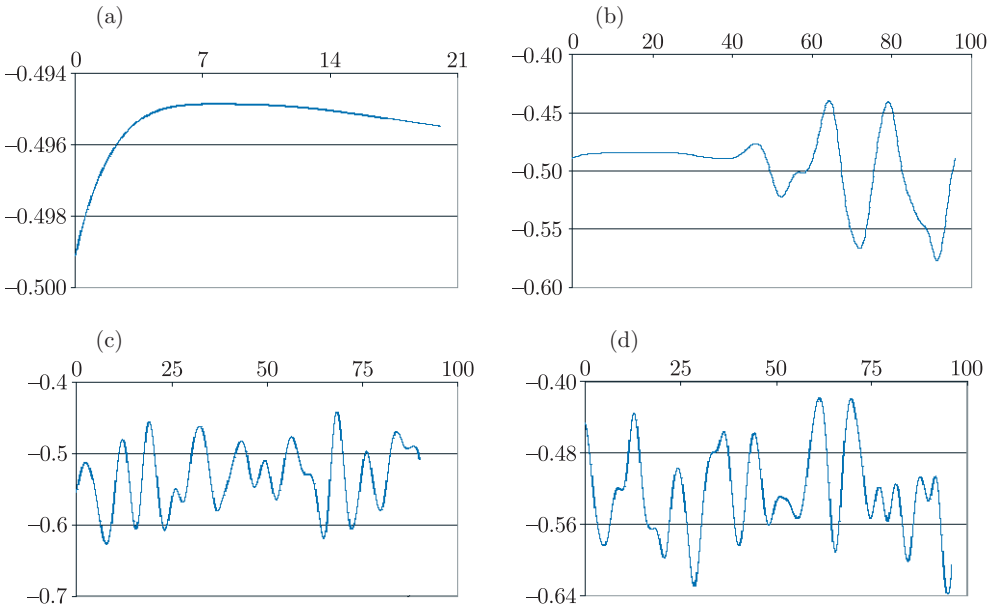

Figure 3. Azimuthal velocity dependence on time for Ro = 1 and (a) Ra = 32 000, (b) Ra = 44 000, (c) Ra = 56 000 and (d) Ra = 80 000 obtained in the stator's middle section

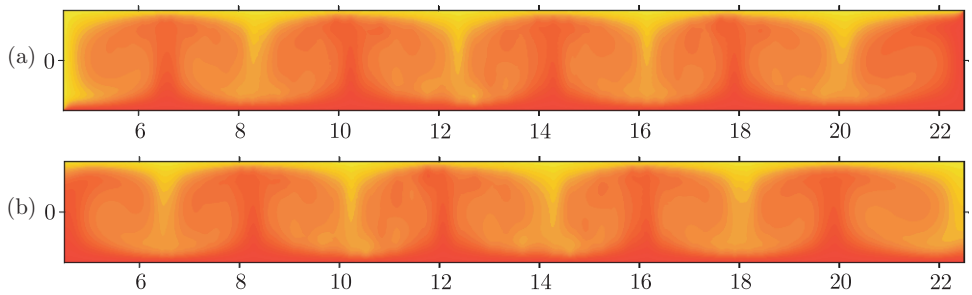

Figure 4. Temperature structure for Ro = 4 and Ra = 44 000: (a) isothermal boundary conditions, (b) adiabatic boundary conditions

$\mathrm{Ro} = 4$, $\mathrm{Ra} = 44\,000$ and for the isothermal and adiabatic boundary conditions at the end-walls is presented in Figures 4a and 4b, respectively. We have clearly observed some kind of a shift in the pattern (Figures 4a and 4b).

6. Conclusions

In this paper, we performed computations using Direct Numerical Simulation method (DNS) based on the pseudospectral collocation Chebyshev-Fourier method. For rotating cavity of $L = 9$ and $\mathrm{Rm} = 1.5$, we investigated the influence of rotation on Rayleigh-Bénard convection. For $\mathrm{Ro} = 1$, 2 and 4, we performed calculations for Ra number from the range $1000 < \mathrm{Ra} < 100\,000$. The results remain in a good qualitative agreement with the results published in the literature. We observed characteristic flow structures reported by many authors – laminar circulation in cells and rolls. We are planning to continue computations for higher Ra values in order to reach chaotic and turbulent state and a study its properties. LES method will be used in future computations.

References

[1] Rossby H T 1969 *J. Fluid Mech.* **36** 309
[2] Siggia E D 1994 *Annu. Rev. Fluid Mech.* **26** 137
[3] Chandrasekhar S 1953 *Proc. R. Soc. Lond.* **A 217** 306
[4] Chandrasekhar S 1961 *Hydrodynamic and Hydromagnetic Stability*, Oxford University Press
[5] Nagakawa Y and Frenzen P 1955 *Tellus* **7** 1
[6] Boubnov B M and Golistyn G S 1986 *J. Fluid Mech.* **167** 503
[7] Zhong F, Ecke R and Steinberg V 1993 *J. Fluid Mech.* **249** 135
[8] Kunnen R P J, Geurts B J and Clercx H J H 2006 *Direct Numerical Simulation of Turbulent Rotating Rayleigh-Benard Convection*, Direct Large-Eddy Simulation VI
[9] Serre E and Pulicani J P 2001 *Computers and Fluids* **30** 491
[10] Tuliszka-Sznitko E and Zieliński A 2006 *J. Theor. Appl. Mech.* **44** (3) 405
[11] Fernando H J S, Chen R-R and Boyer D L 1991 *J. Fluid Mech.* **228** 513
[12] Julien K, Legg S, McWilliams J and Werne J 1996 *J. Fluid Mech.* **322** 243
[13] Vorobieff P and Ecke R E 2002 *J. Fluid Mech.* **458** 191
[14] Zhao A X, Moates F C and Narayanan R 1995 *Phys. Fluids* **7** 1576